Identification of Shielding Material Configurations Using NMIS Imaging*

B. R. Grogan, J. T. Mihalczo, S. M. McConchie, and J. A. Mullens
Oak Ridge National Laboratory, P.O. Box 2008, MS-6010, Oak Ridge, TN 37831-6010, USA
E-Mail Addresses: groganbr@ornl.gov, mihalczojt@ornl.gov,
mcconchiesm@ornl.gov, mullensja@ornl.gov

Abstract

The Nuclear Materials Identification System (NMIS) uses fast neutron tomographic imaging to nonintrusively examine the interior structure of shielded objects. The pixel values in such images represent the attenuation coefficients of the time- and directionally-tagged fast neutrons from a deuterium-tritium (D-T) neutron generator. The reconstruction techniques use either a filtered back projection or a maximum likelihood expectation maximization algorithm. As a first test of the capabilities of these reconstruction techniques to correctly identify individual parts inside of an object, fast neutron imaging was used to identify the regions of shielding surrounding a depleted uranium casting from a library of possible parts. The shielding consisted of multiple regions of common materials such as steel, lead, aluminum, and polyethylene. First, the full object was imaged, and then each of the individual parts was imaged. Several additional parts that were not present in the original object were also imaged to form a library. The individual parts were compared to the full object, and the correct ones were identified using three different methods. These methods included a visual match, an iterative fit of each part, and a mathematical test comparing the sum of squared errors. The successful results demonstrate an initial application of matching. This suggests that it should be possible to implement more sophisticated matching techniques using automated pixel-by-pixel comparison methods in the future.

Introduction

Nuclear Materials Identification System (NMIS) neutron imaging uses the transmission of fast neutrons through an object of interest to reconstruct a tomograph of the object. The transmission detectors are arrayed in a horizontal arc equidistant from the neutron source location, resulting in a one-dimensional map of the number of neutrons passing through the object as a function of angle. If the transmission values are measured with no object in place, the negative natural log of the ratio of the object values divided by the values with no object (void) yields the number of attenuation lengths through the object to each detector. The attenuation length is the product of the path length through the object and the average attenuation coefficient at the energy of the interrogating neutrons. If the object is cylindrically symmetric, or if the object transmission is measured with the target object rotated at several different angles (projections) using a turntable, a two-dimensional (2-D) tomograph of the object at the plane of the detectors can be reconstructed using the known geometry of the source, detectors, and turntable. The pixel values of the reconstruction are the fast neutron attenuation coefficients at each position inside of the object.

By grouping neighboring pixels with a similar attenuation coefficient, simple shapes such as cylinders and boxes can be identified, either visually or by using computational techniques such as the Hough transform [1]. The average attenuation value inside of the shape can be used to tentatively identify its composition. The dimensions of the shapes can then be fitted and combined with the average attenuation coefficients to characterize each individual part inside of the object. If a reference part is available, the reconstructed values can be compared to the reference to determine whether the part inside of the object matches the reference to within the statistical uncertainty of the reconstruction. If a library of potential parts is available, the reconstruction values can be compared with each part in the library to find the best match. In this work, transmission imaging is used to reconstruct an object surrounded by multiple pieces of shielding. A library of potential shielding parts will be constructed, and the parts which form the full object will be matched against the library to determine whether the correct pieces of shielding can be identified.

Measurement Description

The NMIS imaging assembly consists of a neutron source and transmission detectors mounted on a scanning arm. The arm places the neutron source and detectors at the same height, and it moves them up and down synchronously for producing images at multiple heights. The neutron generator is a Thermo-Fisher API-120 [2] deuterium-tritium (D-T) neutron generator. The generator produces approximately 4×10^7 neutrons per second via the $d + t \rightarrow \alpha + n$ reaction. The neutrons are produced isotropically and move away from the alpha particle back-to-back in the center of mass coordinate system. An integral scintillator detects alpha particles in a cone with a half angle of about 25°. The light from the alpha scintillator is transmitted to a Hamamatsu H9500 photomultiplier tube (PMT) [3]. A single row of 16 pixels from the H9500 electronically collimates the neutrons into 16 pixels centered on the horizontal plane of the imaging detectors. The signal from the PMT also provides the start signal for measuring alpha-neutron time coincidences, which correspond to the time-of-flight of the neutron from the source to the detectors. Because the D-T neutrons are monoenergetic, the time-of-flight can be used to eliminate most of the background and scattered neutrons by limiting the transmitted signal to a small time window consistent with neutrons passing directly to the detectors without interaction. The transmission detectors consist of thirty-two $2.54 \times 2.54 \times 10.16$ cm plastic EJ-200 scintillators. The detectors are arrayed in a horizontal fan-beam geometry with the front faces located 115 cm from the neutron source location. To increase the angular resolution, measurements are typically taken multiple times with the detectors shifted slightly between each measurement. This process, known as subsampling, increases the number of effective detector positions, thus increasing the angular resolution of the resulting image.

The object chosen for this set of measurements is a depleted uranium (DU) casting in a cylindrical annulus shape surrounded by two pieces of shielding on the outside and one piece on the inside. The DU casting has an inner diameter of 8.89 cm, an outer diameter of 12.70 cm, and a height of 15.24 cm. The DU contains 0.2% ^{235}U by weight, and it is in a metallic form that has a density of 19.0 g/cm^3. The total mass is 18.7 kg. The DU is sealed inside an annular stainless steel can with an inner diameter of 7.62 cm, an outer diameter of 12.83 cm, a height of 19.05 cm, and a wall thickness of 0.64 mm. The inner piece of shielding is a cylindrical aluminum annulus with an inner diameter of 1.4 cm, an outer diameter of 7.6 cm, and a height of 16.8 cm.

The two outer pieces of shielding are constructed from a series of annular half rings with a height of 2.54 cm. Two sets of half rings are joined together using threaded steel rods which pass through holes drilled near the joining plane. The threaded rods attach to a custom baseplate, which ensures that the alignment of the rings remains constant from one measurement to the next. Seven sets of rings were used for each of the outer regions, yielding an overall height of 17.8 cm. The region immediately outside of the DU can is composed of high-density polyethylene with an inner diameter of 13.4 cm and an outer

diameter of 18.2 cm. The outermost region of shielding is steel with an inner diameter of 18.5 cm and an outer diameter of 23.3 cm. Figure 1 shows the full object configuration.

For this series of measurements, the object was located so that its center was 36 cm from the D-T source location on the line between the source and the center of the imaging detector array. This distance was chosen because it produces good magnification while keeping the entire object well within the ~50° field of view of the detector array. Figure 2 is a diagram of the object location in relation to the neutron generator and imaging detectors. The object was placed on a table so that its base was approximately 63 cm above the level of the floor. The attenuation through the object was measured at 71 cm above the floor, near the vertical center of the DU annulus, to reduce any edge effects near the top or bottom. Each measurement was divided into four subsamples to produce 128 effective detector positions. Because the object and its parts were cylindrically symmetric, only a single projection was performed for each. This was done primarily in the interest of time; however, multiple projections would be required for an unknown object if cylindrical symmetry could not be assumed.

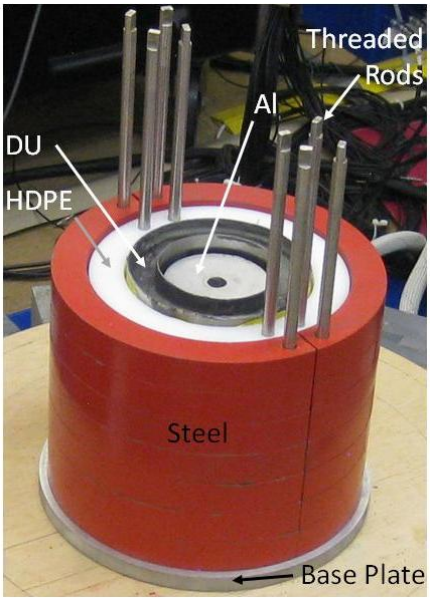

Figure 1. The fully assembled object consists of four cylindrical annuli composed of aluminum, DU, high-density polyethylene, and steel. The threaded rods and custom baseplate ensure that the individual parts are aligned in the same manner for each measurement.

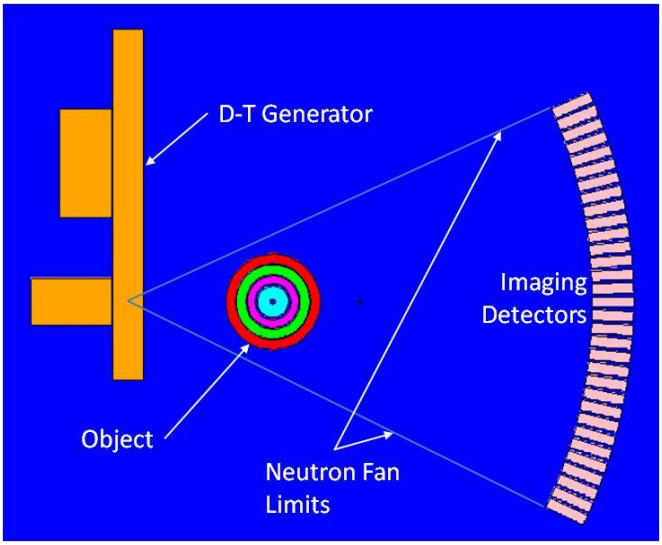

Figure 2. The configuration of the D-T generator, imaging detectors, and object. The two lines showing the fan beam limits converge at the approximate location of neutron production inside of the generator. This point is located 36 cm from the center of the object and 115 cm from the front faces of the imaging detectors.

After a void measurement of 40 minutes (4 subsamples of 10 minutes each), the full object was measured for 60 minutes. After the full object, each of the four parts was measured individually for 60 minutes. The parts were measured at the same location they occupied in the full object using markings on the baseplate or the threaded rods for alignment. In addition, five other parts which were not in the assembled object were measured for 60 minutes each. Each of these parts had identical dimensions to one of the correct pieces of shielding but was composed of a different material. The materials selected had attenuation coefficients which differed enough that it would be possible to distinguish one from another. These nine parts, four of which were in the assembled object, formed the library of parts from which the shielding would be identified.

Analysis and Results

After the measurements were completed, attenuation maps of the full object and each of the individual parts were computed. With NMIS measurements, one of two methods is typically used to reconstruct the attenuation curves into a 2-D tomograph of the attenuation coefficients. The first method uses a simple filtered back projection (FBP). This reconstruction method has been used in the imaging community for many years because it is extremely fast computationally. Unfortunately, the speed comes at the cost of imaging quality. FBPs typically show artifacts and streaking caused by statistical fluctuations in the data. To overcome this shortcoming, FBP images are processed by the TAKE algorithm, which performs an iterative fit using ray tracing. The operator identifies simple shapes such as cylinders or boxes and inputs an initial model into the TAKE algorithm based on the FBP results. During each iteration, the TAKE algorithm generates an attenuation curve based on the model, compares it to the measured attenuation curve, and then adjusts the model parameters based on the differences. Typical parameters that can be fit are the x and y positions of the center of each shape, the attenuation coefficient, and the dimensions. At the end of the TAKE algorithm, the best-fit values for each of these parameters are returned to the user. Currently the identification of each shape is done manually, but future improvements should allow for an automated method for identifying shapes. Figure 3(a) shows the original FBP of the full object and Figure 3(b) the resulting TAKE fit.

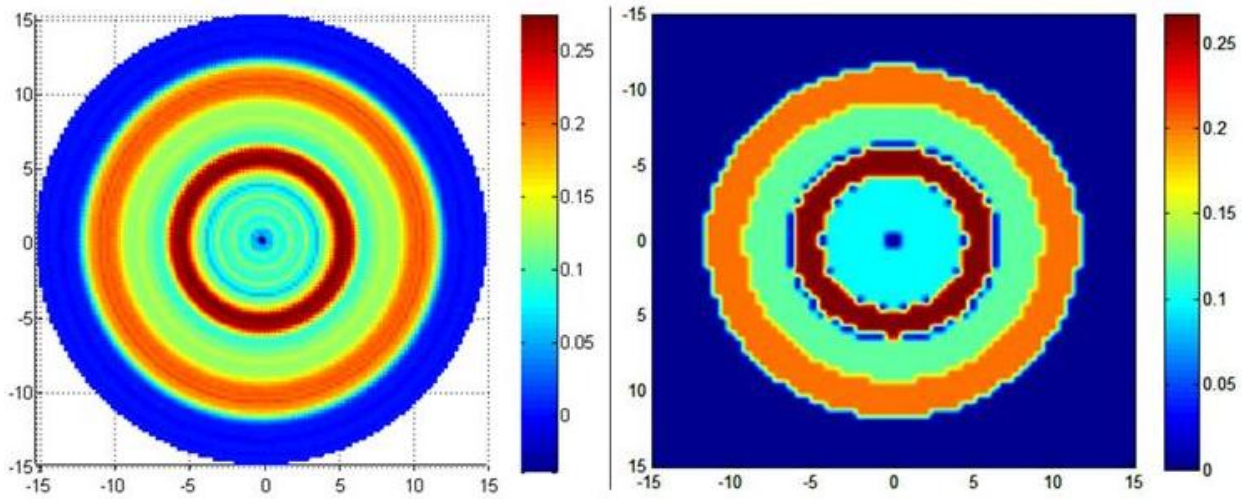

Figure 3. The FBP reconstruction of the full object (a) and the TAKE fit of the FBP data (b). The TAKE fit smoothes out the rotational artifacts which are present in the FBP and assigns a single attenuation coefficient to each region.

For the FBP-TAKE method, the images of the nine individual parts and the assembled object were reconstructed and fitted. The values for the initial guesses were estimated by examining the FBP of the assembled object. The same guess was used for each of the individual parts for consistency—the TAKE algorithm quickly discarded the regions which were clearly not present. Table 1 shows the fit results for each of the regions of the object. The fitted parameters (inside diameter, outside diameter, and attenuation coefficient) of each region in the assembled object are compared to each of the parts in the library. The highlighted rows represent the four individual parts which were present in the full object. For each of the three parameters, the fractional error was calculated by dividing the difference between the two values by the value from the full object reconstruction. The total fractional error was computed by summing the three terms in quadrature. Note that for each region, the correct part was the one with the lowest total fractional error, indicating a successful match.

Table 1. Comparison of TAKE Fit Parameters Showing the Fractional Errors of the Differences

Assembled Object				Individual Parts from the Library				Fractional Errors of the Differences[a]			
Region	ID (cm)	OD (cm)	Coeff. (cm^{-1})	Part	ID (cm)	OD (cm)	Coeff. (cm^{-1})	ID	OD	Coeff.	Total
1	18.65	23.60	0.199	11	18.91	23.75	0.110	0.014	0.006	-0.445	0.445
				12	18.43	23.62	0.198	-0.012	0.001	-0.003	0.012
				13	18.80	23.74	0.151	0.008	0.006	-0.242	0.243
2	13.62	18.65	0.127	21	13.67	18.56	0.111	0.004	-0.005	-0.126	0.126
				22	13.35	18.66	0.189	-0.019	0.000	0.495	0.496
				23	13.49	18.59	0.156	-0.009	-0.003	0.228	0.228
3	8.69	12.81	0.257	34	8.45	12.88	0.239	-0.028	0.005	-0.070	0.075
4	1.16	8.00	0.097	41	1.22	7.79	0.101	0.054	-0.026	0.044	0.074
				42	1.26	7.75	0.212	0.092	-0.031	1.178	1.182

[a]Calculated by dividing the difference between the two values (region and individual part) by the value from the full object reconstruction. The total fractional error was computed by summing the three terms in quadrature.

Note: The correct part for each region is shaded. For each region, the correct part had the lowest total fractional error.

Abbreviations: ID = internal diameter, OD = outer diameter, and Coeff. = attenuation coefficient.

The second image reconstruction technique uses a maximum likelihood expectation maximization (MLEM) algorithm. The MLEM algorithm begins by guessing the attenuation coefficient of each pixel in the field of view of the reconstruction. Here, a value of 1 is assigned to each pixel as the initial guess. For each detector position, the sum of the attenuation coefficients multiplied by the path length of each pixel along the path is forward projected to form a sinogram. The ratio of this guessed attenuation sinogram to the measured values forms a correction term which is back projected onto each pixel. This process is iterated until a well-converged image is formed. For all reconstructions performed in this work, 50 iterations were used.

When the individual parts were reconstructed using the MLEM algorithm, their reconstructions were summed to produce a possible composite object. One part from the library was used for each of the four regions of the object. All 18 possible configurations of parts (3×3×1×2) were constructed in this manner. Each of these was then compared to the fully assembled object to determine the one that matched best. All 18 configurations and the fully assembled object are shown in Figure 4.

The first method used for comparing the composite images to the full object used simple visual identification. The set of images shown in Figure 4 was given to five students who were asked to select the configuration that best matched the full object. These students all had some level of familiarity with neutron imaging reconstructions but no affiliation with this particular measurement or the actual object used. All five students were able to correctly identify configuration (composite object) 7 as the set of objects used in the full object. As a follow-up question, each student was also asked if he or she could identify the materials in the assembled object. Although none got the exact materials correct, all of the incorrect guesses involved materials with attenuation coefficients very close to the materials used (e.g., guessing aluminum for the polyethylene region).

The second method for comparing the composite objects to the full object used the sum of squared errors (SSE). The SSE for each configuration was computed using the equation

$$SSE = \sum_{i=1}^{N} \sum_{j=1}^{N} O_{i,j} - C_{i,j}^{\ 2},$$

where *i* and *j* are indices of the horizontal and vertical pixels, *N* is the number of pixels in the image in each direction, *O* is the reconstructed attenuation coefficient value in the full object image, and *C* is the attenuation coefficient value in the composite object being tested. Table 2 shows the SSE value for each of the composite configurations. As with the visual identification test, the SSE correctly selected configuration number 7 as the best match to the full object.

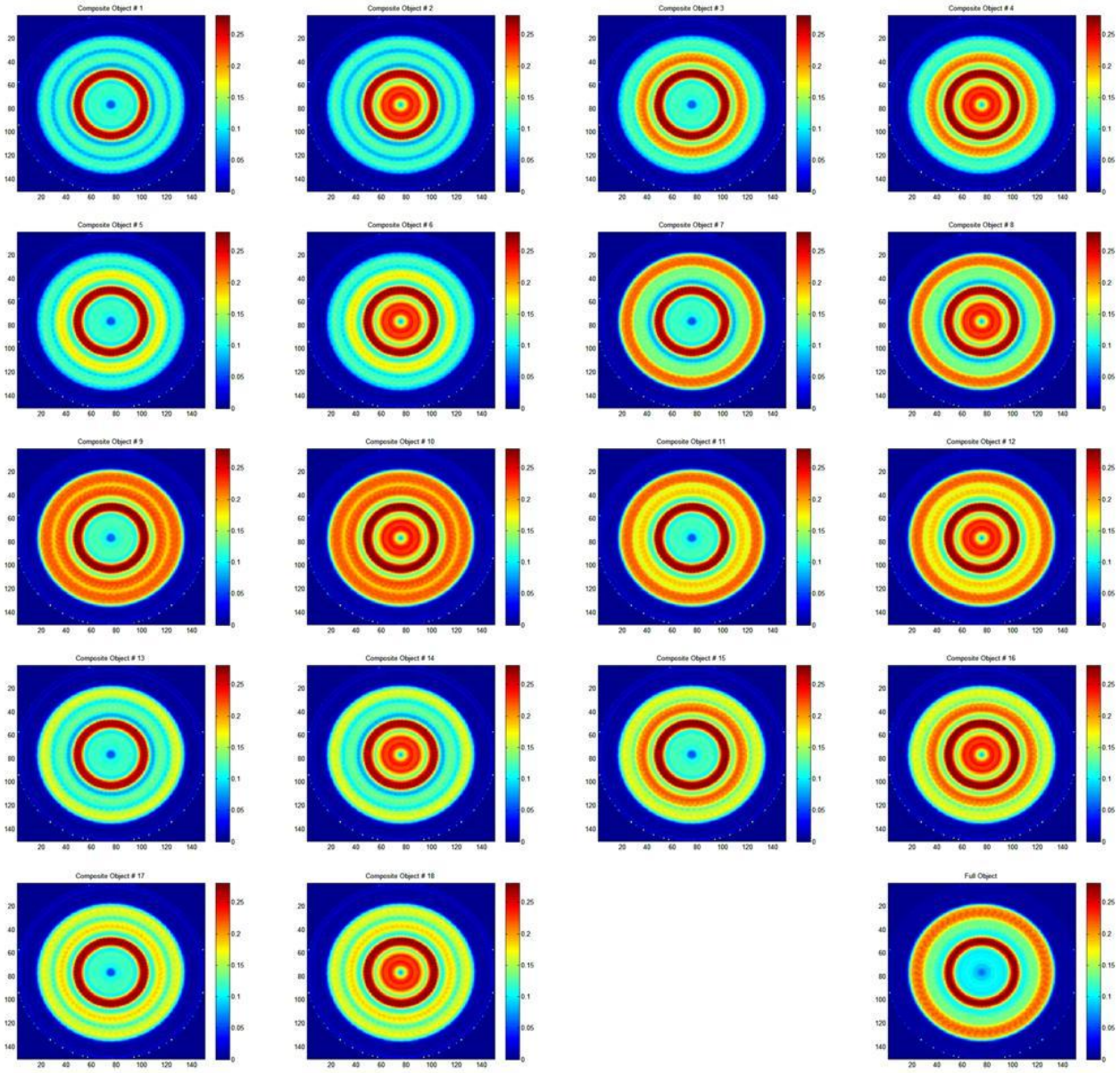

Figure 4. MLEM reconstructions of each of the eighteen possible configurations of the nine parts in the library and the MLEM reconstruction of the full object at the bottom right. The configuration containing the correct parts is composite object 7, which is the second from the right on the second row.

Table 2. SSE Results for Each of the 18 Composite Object Configurations

Configuration	SSE	Configuration	SSE
1	34.93	10	34.17
2	48.91	11	6.28
3	40.84	12	21.28
4	55.61	13	13.60
5	33.53	14	27.83
6	47.78	15	24.03
7[a]	1.43	16	39.05
8	16.16	17	14.73
9	18.65	18	29.22

[a]Configuration 7 consisted of the correct parts and had the lowest SSE of all configurations.

Conclusions and Future Work

This work has shown that tomographic reconstructions of fast neutron measurements made with NMIS can be used to successfully identify individual parts of an object from a library of possible parts. Each of the three methods used correctly selected the three pieces of shielding around the DU annulus in the full object. While somewhat trivial, this exercise was necessary to validate the method using a simple scenario before proceeding to more complex ones and to determine the specific areas where future efforts need to be concentrated.

Presently, there are two methods for reconstructing neutron tomographs with NMIS imaging. Each method has its advantages and disadvantages, but ideally these two can be combined into a single reconstruction algorithm. In particular, the FBP-TAKE method relies, to some extent, on the identification of the correct number of parts by the operator, but it provides exact values of the fit parameters at the conclusion. The MLEM algorithm, on the other hand, uses a general guess for all reconstructions, but there is no method at this time for identifying shapes or extracting the parameters of each one. Application of an automatic shape-recognition algorithm such as a Hough transform to the MLEM results could accomplish this. Finally, for more complex shapes, an image registration technique which can pick out shapes on a pixel-by-pixel basis will be needed to correctly identify parts that have been translated or rotated from their original position in the full object. If successfully implemented, these additional capabilities could allow NMIS imaging to identify complex parts which have been removed from an object and placed randomly in another container.

References

1. D. H. Ballard, "Generalizing the Hough Transform to Detect Arbitrary Shapes," *Pattern Recognition*, **13**, 111–122 (1981).

2. Thermo Scientific API 120 Neutron Generator, http://www.thermoscientific.com/ecomm/servlet/productsdetail_11152_L10445_82242_11962775_-1 (accessed May 2011).

3. Hamamatsu H9500 Photomultiplier Tube Module, http://sales.hamamatsu.com/en/products/electron-tube-division/detectors/photomultiplier-modules/part-h9500.php (accessed May 2011).